

gärtner [*Phys. Rev. Lett.* 63, 1324 (1989)], which increases our confidence that true thermodynamic equilibrium has been achieved.

15. This linearity breaks down far from the center, due to violent fluctuations of the membrane boundary. This boundary curls up significantly even in the flat phase, leading to contributions to a diffuse in-plane interface at this boundary which scale like  $L^5$  and  $L^{\omega 2}$ . See (13).
16. For a discussion of possible experiments, see D. R. Nelson, in *Statistical Mechanics of Membranes and Inter-*

faces, D. R. Nelson, T. Piran, S. Weinberg, Eds. (World Scientific, Singapore, 1989).

17. We thank W. E. Rudge for the graphics of Fig. 1. We have benefited from conversations with I. P. Batra, G. Grest, Y. Kantor, M. Kardar, and M. Plischke. Research by D.R.N. was supported by the National Science Foundation, through grant DMR88-17291 and through the Harvard Materials Science Laboratory.

6 March 1990; accepted 16 May 1990

## Evolution of the Northern Santa Cruz Mountains by Advection of Crust Past a San Andreas Fault Bend

ROBERT S. ANDERSON

The late Quaternary marine terraces near Santa Cruz, California, reflect uplift associated with the nearby restraining bend on the San Andreas fault. Excellent correspondence of the coseismic vertical displacement field caused by the 17 October 1989 magnitude 7.1 Loma Prieta earthquake and the present elevations of these terraces allows calculation of maximum long-term uplift rates 1 to 2 kilometers west of the San Andreas fault of 0.8 millimeters per year. Over several million years, this uplift, in concert with the right lateral translation of the resulting topography, and with continual attack by geomorphic processes, can account for the general topography of the northern Santa Cruz Mountains.

**A**LTHOUGH THE GENERAL PATTERN of strain expected around restraining bends in strike-slip faults has long been known to result in uplift near the bend (1), the long-term dynamics of this uplift have rarely been documented. Strain patterns associated with strike-slip faults vary with the bend geometry, and with the slip distribution along the fault (2). Uplift rate maxima should coincide with the center of restraining bends, and die away from these bends in all directions. The combination of fault planes that accommodate the areal strain is not often known, however. As in the dip-slip fault case (3), a full model for the development of fault bend-related topography must necessarily include the patterns of coseismic uplift, interseismic relaxation, and geomorphic redistribution of mass. An added complexity in the strike-slip case results from the long-term advection of the evolving topography relative to the bend (4). The resulting topography rises in altitude when the local rate of uplift exceeds the rate of lowering due to geomorphic processes and decays when the geomorphic lowering dominates.

The Santa Cruz Mountains provide an excellent location for the study of fault bend dynamics because we may infer long-term uplift rates from well-dated marine terraces, the fault geometry and slip rates are well constrained, a recent seismic uplift event has

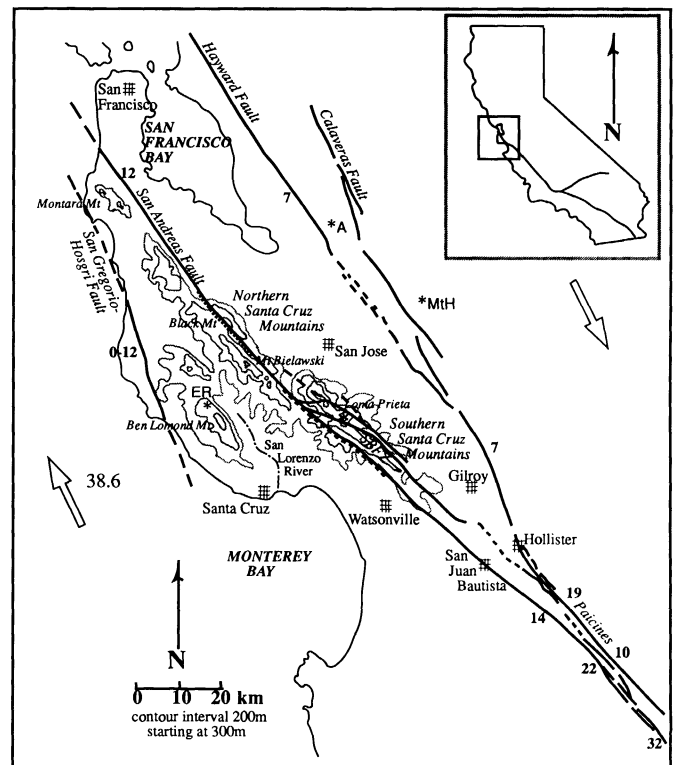
occurred [the magnitude ( $M_s$ ) 7.1 Loma Prieta earthquake of 17 October 1989 (5, 6)] from which the coseismic uplift pattern may be inferred, and the geomorphic denudation rates are available. In this paper, I show that the time scales and magnitudes of

the tectonic and geomorphic processes are consistent with the present topography of the Northern Santa Cruz Mountains. Both the topography that fits this simple picture, and that which does not, have implications for long-term slip rates, repeat times, the occurrence of other seismic events, and the longevity of bends in this reach of the San Andreas fault system.

Locally, the San Andreas fault (SAF; Fig. 1) slips at a rate of  $12.2 \pm 3.9$  mm/yr (7, 8). The fault bends at several different scales in the Santa Cruz Mountains (9). In the region between San Juan Bautista and the northern San Francisco peninsula the SAF describes a broad bend with a wavelength of 100 km (Fig. 1). This bend is accomplished by several shorter bends with divergence angles of  $8^\circ$  to  $10^\circ$  and wavelengths of  $\sim 10$  km. One of these ( $10^\circ$ ) is centered north of Santa Cruz, the other at Black Mountain ( $8^\circ$ ) just west of Los Altos Hills (Fig. 1). The rupture associated with the Loma Prieta earthquake was centered about the first of these bends.

The Santa Cruz Mountains hug the SAF for  $\sim 100$  km (Fig. 1). The fault crosses the middle of the mountain range in a prominent double restraining bend of approximately 3 km amplitude and 10 km length; the northern range occurs west of the fault and the southern range occurs to the east. The highest topography in the northern range (Mount Bielawski, 985 m) occurs near the northern edge of this bend, whereas

**Fig. 1.** Map of the Santa Cruz Mountains surrounding the slight bend in the San Andreas fault (SAF) in which the recent 17 October 1989 earthquake nucleated, as well as other major faults in the area (slip rates shown in millimeters per year; SBFZ, Sargent-Berrocal fault zone). Index map shows the SAF as it passes through California, and the Garlock fault. Note the broad bend in the SAF in the Monterey Bay region separating straight reaches of the fault. Smaller bends are the Santa Cruz bend, (long dashed) and the Black Mountain bend (short dashed). Topographic contours are shown at 200-m intervals starting at 300 m. Other topography (to the east of San Francisco Bay, and on the Monterey Peninsula) is not shown. Asterisks denote positions of geodetic stations occupied by the U.S. Geological Survey in the aftermath of the Loma Prieta earthquake.



Earth Sciences Board, University of California, Santa Cruz, CA 95064.

that in the southern range occurs roughly in the middle (Loma Prieta, 1185 m). Both the topographic crest and the vertical cross-sectional area of the mountain ranges decrease essentially monotonically with distance away from the bend in the direction of plate motion; the length scale for decay is ~50 km for the northern range, 30 km for the southern. The topographic crest lies consistently 1.5 to 2 km away from the trace of the fault, and the range is steepest on the fault-facing side.

Four to six marine terraces grace the Santa Cruz coastline (Fig. 2) (10–14). These provide an opportunity to assess the cumulative uplift pattern over several hundred thousand years, as the altitudes of the inner edges of the wavecut platforms underlying the terraces may be taken to represent ancient mean sea level. Recently refined global sea level curves allow ages to be assigned to the terraces with considerable certainty (10, 12, 15–18) (Table 1). In addition, the uplift pattern normal to the coast is revealed in transects 10 to 20 km northwest of Santa Cruz. Here, wavecut platforms of increasing age display increasing seaward tilt; the rate of westward tilting is ~0.5° per million years (10).

Data collected during and after the  $M_s$  7.1 Loma Prieta earthquake of 17 October 1989 shed considerable light on the nature of the San Andreas dextral transform boundary in this region (5). The focal mechanism of the main shock consisted of both right lateral and reverse motion. Aftershocks occurred in a zone ~40 km in length and from ~18 to 5 km in depth (6, 19). The locus of aftershocks define a narrow ~70° southwest dipping plane at depth and a more diffuse but generally more vertical

**Table 1.** Terrace names, ages (ka, thousand years ago), isotope stages, and altitude of original formation.

Terrace	Age (ka)	Isotope stage	Altitude (m)
Santa Cruz	81, 105	5a, 5c	-19, -9
Cement	120	5e	+6
Western	212	7a	-7
Wilder	330	9a	+4
Black Rock	500	13?	0?
Quarry	610	0?	

zone near the surface (20). Geodetic data show that ~1.7 m of strike slip and 1.2 m of thrust motion occurred (6, 20). The calculated uplift pattern (Fig. 2) reveals that maximum uplift of 0.55 m occurred parallel to the fault and ~2 km to the southwest of it (21). Models based on these data suggest that slight subsidence of up to 0.15 m should have occurred to the northeast of the fault trace, centered over the eastern flank of Loma Prieta Ridge.

Consider a coordinate system (Fig. 2) established with  $x$  parallel to the fault in the direction of Pacific plate motion,  $y$  perpendicular to the fault, and  $z$  vertical. For an uplift rate pattern  $D(x, t)$  that is fixed in space and constant in time,  $t$ , the spatial distribution of uplift,  $z(x, t)$ , is obtained by integrating the uplift rate as seen by a parcel of landscape traveling with the long-term slip velocity,  $U$

$$z(x, t) = \frac{1}{\tau_r} \int_0^t \delta z(x - Ut') dt' + z(x, 0) \quad (1)$$

where  $D(x, t)$  is replaced by  $\delta z(x)/\tau_r$ , where  $\delta z(x)$  is the uplift per earthquake for a characteristic event that it is repeated identi-

cally many times (22),  $\tau_r$  is the repeat time for such events, and  $z(x, 0)$  is the initial topography. The marine terraces allow two important simplifications. First, the initial topography may be taken to be the formation altitude of the platform everywhere, a proper assumption if all elevations are referenced to the inner edges of the wavecut platforms. Second, in the 81,000 to 212,000 years since their formation (Table 1), the most prominent terraces (Santa Cruz, Cement, and Western) should have translated 1 to 3 km to the northwest because of slip along the SAF. As this is only a small part of the ~40 km strike-parallel width of the single event uplift pattern (Fig. 2), the contribution of the advective part in Eq. 1 is minimal; it may therefore be rewritten

$$z_t(x) = \frac{\tau_t}{\tau_r} \delta z(x) \quad (2)$$

where  $\tau_t$  is the age of the particular terrace and  $z_t$  is its present inner edge elevation less its initial formation altitude (that is, the total uplift). Therefore, if the uplift pattern inferred from the Loma Prieta event,  $\delta z(x)$ , is characteristic, then this pattern should closely correspond to the pattern of total uplift for any particular marine terrace,  $z_t(x)$ ; furthermore, knowing the terrace age, we may infer repeat times. The two patterns do correspond closely (Fig. 3) to the south of Santa Cruz, but diverge to the north, where the terrace elevations are above those predicted. The Greyhound Rock arch (10) (Fig. 3) represents the most glaring deviation.

The elevations of the marine terraces between Santa Cruz and Watsonville may thus be simply explained by uplift caused by repeated Loma Prieta-like earthquakes. The consistent increase in seaward platform tilt with age further supports this conclusion. The implied repeat time,  $\tau_r$ , calculated from Eq. 2 is 660 to 720 years. The implied maximum uplift rate in the center of the uplift pattern is 0.80 mm/yr (0.55 m/690 yr). The uplift pattern associated with the Loma Prieta event is as yet unverified in the far field, that is, along the coast. Although the amplitude of the uplift pattern is sensitive to assumptions made in the calculation, the shape of the pattern is most likely robust, as it is controlled by the fault geometry; as a consequence, the calculated repeat times will likely change only slightly.

The excess elevation of the terraces to the north of Santa Cruz requires the operation of another agent in addition to repeated Loma Prieta events. Although activity on the nearby San Gregorio fault zone (15) could be the cause, the monotonic increase in seaward tilt with terrace age (10) implies that uplift is centered about the SAF.

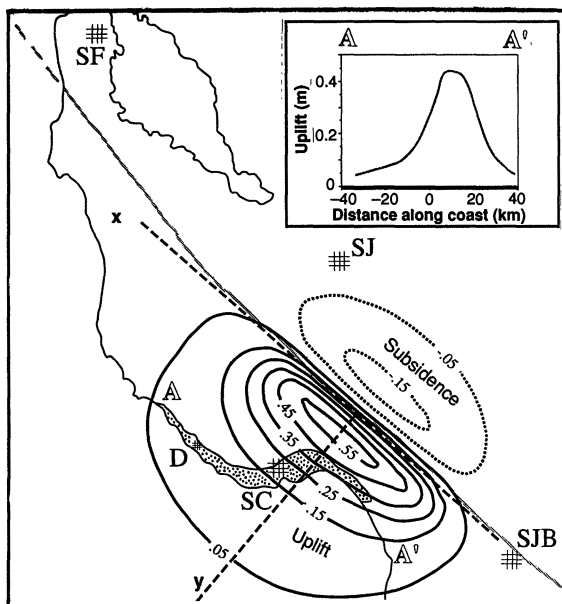


**Fig. 2.** Pattern of uplift along the fault on same scale as Fig. 1, (see references in text). Isolines of uplift in meters. Note slight subsidence on the North American plate east of the SAF near the highest part of the southern Santa Cruz Mountains. The shaded region along the coast depicts marine terrace deposits. Inset shows predicted uplift along a transect A-A' paralleling the coast at the location of the inner edge of the first terrace. Also shown is the coordinate system for calculation of total uplift patterns. Not depicted,  $U$  is the advection velocity, positive in the  $+x$  direction; and  $z$  is vertical (elevation); SC, Santa Cruz; SF, San Francisco; SJB, San Juan Bautista.

If the model of the marine terraces is correct, then the larger scale features of the landscape should also correspond to the coseismic uplift pattern. Advection of the tectonically generated topography relative to the bend, geomorphic attack, and long-term accommodation of the load imposed by the growing topography will modify the landscape and must be considered.

The total coseismic uplift is related to the spatial pattern of coseismic uplift,  $\delta z(x, \gamma)$ , the advection velocity,  $U$ , and  $\tau_r$ . The elevations created by translation entirely through this uplift pattern may be assessed by treating the steady-state case of Eq. 1. The total uplift at any point along a path of constant distance,  $\gamma$ , from the fault becomes

$$z(x, \gamma) = \frac{1}{U\tau_r} \int_{-\infty}^x \delta z(x', \gamma) dx' \quad (3)$$

I assume that there is no initial topography and that the slip velocity and the uplift pattern have been constant in time.

A reasonable fit to the calculated uplift pattern (Fig. 2) at any fixed distance from the fault,  $\gamma$ , is obtained with a normal distribution  $\delta z(x, \gamma) = \delta z_0(\gamma) \exp[-(x/\sigma)^2]$ , where  $\delta z_0(\gamma)$  is the amplitude of the pattern, which varies with distance from the fault, and  $\sigma$  is the length scale of the pattern in the direction of relative plate motion. Integration through the entire uplift pattern yields an expected maximum tectonic elevation of

$$z_{\max}(\gamma) = \frac{\sqrt{\pi} \sigma \delta z_0(\gamma)}{U\tau_r} \quad (4)$$

At a distance of 2 km southwest of the

fault trace ( $\gamma = 2$  km), corresponding to both the northern Santa Cruz Mountain crest and the uplift maximum,  $\delta z_0 = 0.55$  m and  $\sigma = 25$  km (Fig. 2). The maximum expected elevation, for a slip rate of 12.2 mm/yr and an average repeat time of  $\sim 700$  years, is about 2800 m. The elevation of Mount Bielawski is  $\sim 1000$  m. This estimate is sensitive to  $U$ ,  $\tau_r$ , which is directly proportional to the magnitude of the uplift pattern, and  $\sigma$ . However, combination of Eqs. 2 and 4 demonstrates that the calculation is sensitive only to the ratio of uplift at the two locations,  $\delta z_0/\delta z_t$ , and should therefore be less sensitive to future revelations of measured uplift pattern magnitude.

Can the 1800-m discrepancy be accounted for by a combination of isostatic deflection and geomorphic processes? Isostatic compensation should have taken place during the 4 million years necessary to translate crust through the bend, as compensation times are of the order of 1000 to 2000 years (23–25). If the Santa Cruz Mountains are approximated as a 50-km-wide line load oriented parallel to the San Andreas of initial height 1800 m the expected deflection is  $\sim 700$  m (26). This brings the expected topographic maximum down from 2800 to 2100 m.

North of the point where the tectonic uplift rate equals the decay rate due to geomorphic processes, the ridge crest elevation should decline monotonically with distance. The scale for the decay rate is set by the efficiency of the processes, which may be

constrained by two independent measurements: (i) the modern sediment fluxes from streams draining the mountains, and (ii) the decrease of the cross-sectional area of the mountain range with time (distance). Sediment transport measurements and calculations (27, 28) for the San Lorenzo basin, the largest in the area (roughly 352 km<sup>2</sup>), indicate that mean basin-averaged lowering rate is  $\sim 0.27$  mm/yr; the rate for the Pescadero basin (154 km<sup>2</sup>) is 0.22 mm/yr, and the rate for the San Gregorio basin (139 km<sup>2</sup>) is 0.30 mm/yr.

If there is no further tectonic forcing along this reach of the fault and if both slip rates and geomorphic processes have remained both uniform in space and constant in time for the last 4 million years, then the topography of the northern range (Fig. 4) suggests that the decay rate of the range cross section is 3 km<sup>2</sup> per million years. Dividing by the width of the mountain range perpendicular to the fault yields a long-term mean denudation rate of  $\sim 0.2$  to 0.3 mm/yr, in good accord with the modern rates. Undoubtedly these average rates are underestimates of the rates of crest decline, as surficial processes are enhanced with both elevation and slope.

Erosion may therefore account for several hundred meters of elevation decrease during the 4 million years needed to translate topography through the 50-km-wide uplift pattern. Therefore, the sum of the coseismic forcing ( $\sim 2800$  m), the mantle relaxation ( $\sim 700$  m), and the geomorphic processes ( $\sim 1000$  m) reasonably result in the 1000-m maximum crest heights seen in the northern Santa Cruz Mountains.

The predicted uplift pattern cannot account for the present elevation of the southern Santa Cruz Mountains, dominated by Loma Prieta Ridge, which is 200 m higher than the highest topography in the northern range and is centered east of the Santa Cruz bend on the subsidence part of the vertical displacement pattern based on the Loma Prieta earthquake (compare Figs. 1 and 2). Other uplift mechanisms must therefore occur that not only undo the subsidence caused by repeated Loma Prieta events, but produce positive topography at a rate great enough to counter geomorphic erosion as well. That the maximum topography on the North American side of the fault is at the center, rather than the edge, of the bend implies that the east side of the fault is advecting relative to the bend more slowly than the west. One additional uplift mechanism may be repeated events on the Sargent-Berrocal fault system (SBFZ on Fig. 1) (29) which shows evidence of both thrust and dextral strike-slip motion (30–33). Oblique motion on the southwest dipping Sargent

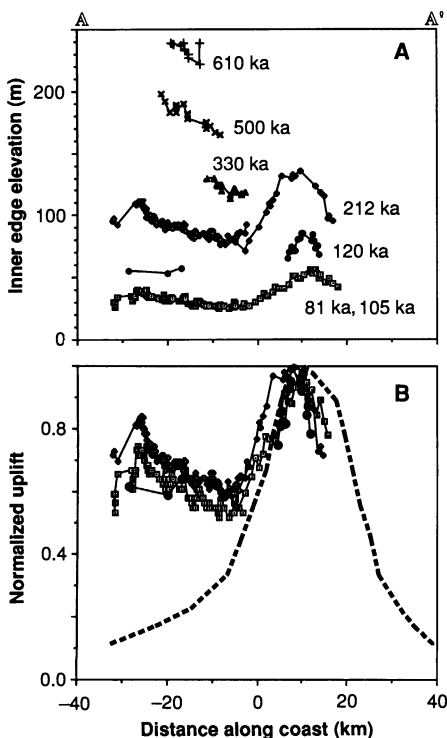


**Fig. 3.** (A) Terrace elevations through the study area (see text and Table 1 for references and names). All elevations taken at the inner edge of the wavecut platform (10, 11). The terraces all reach a peak elevation in the region of Aptos,  $\sim 8$  km south of the mouth of the San Lorenzo River (Fig. 1), and display a second maximum well to the north, at the Greyhound Rock arch (10). Note the slight shift of terrace elevation maxima to the northwest with age, as expected from right lateral slip on the SAF. (B) Patterns of total uplift at the wavecut platform inner edges [difference between present elevations (A) and formation elevations (Table 1)], and Loma Prieta uplift (Fig. 2, inset), each normalized with respect to its maximum value to facilitate comparison. The patterns overlay neatly in the region south of Santa Cruz.

fault would both accomplish the proper uplift pattern and reduce the long-term slip of the resulting topography with respect to the bend.

The proposed recurrence interval of 700 years for uplift events based on vertical displacement patterns is much longer than that calculated using right lateral offset. A 12.2 mm/yr slip rate (8), and the right lateral offset of 1.7 from the Loma Prieta earthquake (5, 6), implies that repeat times are ~150 years. Either the magnitude of the inferred uplift pattern is greatly in error, or, more likely, other events accomplish right lateral strike slip while not adding significantly to the elevation of the coastal terraces. Obviously, 1906-type events also accomplish dextral slip [of order 1 to 2 m in this reach of the fault, down sharply from the 4 m to the northwest (34)]. Little is known about the vertical deformation patterns associated with these great earthquakes in the Santa Cruz Mountains. Local bend-related events may be responsible for the accommodation of the slip deficit in this region created by 1906-type earthquakes. That the slip along this portion of the SAF is accomplished by a variety of events is not unlike the complex behavior of other fault zones around the Pacific Rim (35).

Several possible alternative explanations for the pattern of the Santa Cruz Mountains topography include: preexisting topography now juxtaposed across the fault; differences in lithologic resistance to erosion; topography produced by a more complex bend than

modeled; the result of compression across the fault on a broader scale; or some combination of the above mechanisms. If the Santa Cruz Mountains result from regional compression associated with coast ranges deformation (36), and have since been sliced by the SAF, then the northern and southern ranges must now be fortuitously juxtaposed. Further support that the elevation of the coastal terraces reflects events on the bend in the SAF (37) is the 4° seaward tilt of the unconformity between Salinian basement and ~8- to 10-million-year-old sediments (38). These relations imply a mean tilt rate of ~0.4° to 0.5° per million years, in close accord with the measured tilt rate of the terraces.

I have ignored the effects of events centered farther north along the trace of the SAF. The elevation of Black Mountain, which cannot be accounted for in the proposed scenario, is perhaps due to repeated earthquakes centered around the Black Mountain bend. Indeed, one scenario for the anomalous elevation of the terraces north of Santa Cruz (the Greyhound Rock arch) is that this represents the far field effects of the uplift associated with such events. I have not taken into account the effects of nonuniform strike slip on the SAF; nonuniform slip can significantly affect uplift patterns (2). Nor have I rigorously addressed the geomorphic issues. The hillslope processes acting are dominated by landsliding in a steep, forested landscape, the rates of which are controlled by the rates of

incision of a complex arborescent stream system, each segment of which defines the lower boundary conditions for the adjoining hillslope (39).

Although the calculations have been based upon the assumption that Loma Prieta-type events are the sole source of uplift to the west of the SAF, it is likely that the terrace elevations reflect a combination of types of seismic events. While the operation of other such events will alter the calculated repeat time of Loma Prieta events, the quantitative model of the growth of the northern Santa Cruz Mountains is sensitive only to the assumption that each of these events results in a maximum uplift near the fault. The maximum uplift rate of 0.8 mm/yr is obtained from the product of the uplift rate at the inner edge of a terrace (total terrace uplift divided by terrace age) and the ratio of the uplift near the fault with that at the inner edge. Although the ratio used is based upon the Loma Prieta event, it is likely that most coseismic uplift patterns resulting from movement through the fault bend are broadly similar (40).

In general, the model, even if incorrect in detail, shows that the topography of a restraining bend-related mountain range, when combined with available geologic data, can be used to constrain possible models for the dynamics of the bend. Over long times, advection relative to the bend of the topography resulting from combined coseismic, interseismic, and geomorphic processes must be taken into account. The evolution of the mountain range cross section and of the drainage system provides a data base for the assessment of long-term rates of geomorphic processes, and can in addition serve as a check on the relevance of modern measurements of geomorphic processes. From the tectonic perspective, the topography can potentially augment geological information in the construction of dynamic models for particular restraining bends, within which the operation of one or several discrete slip planes must accommodate the geometrically required areal strain. From the seismological perspective, the topography serves as an important test for hypothesized, potentially quite complex seismic event scenarios operating over long time spans. If coseismic deformation fields are available, long-term average repeat times for seismic events may be inferred from preserved paleohorizontal markers in the form of marine terraces, lake shorelines, or erosional unconformities.

#### REFERENCES AND NOTES

1. See review by A. G. Sylvester, *Geol. Soc. Am. Bull.* 100, 1666 (1988).
2. These are modeled by R. Bilham and G. C. P. King, *J. Geophys. Res.* 94, 10204 (1989).

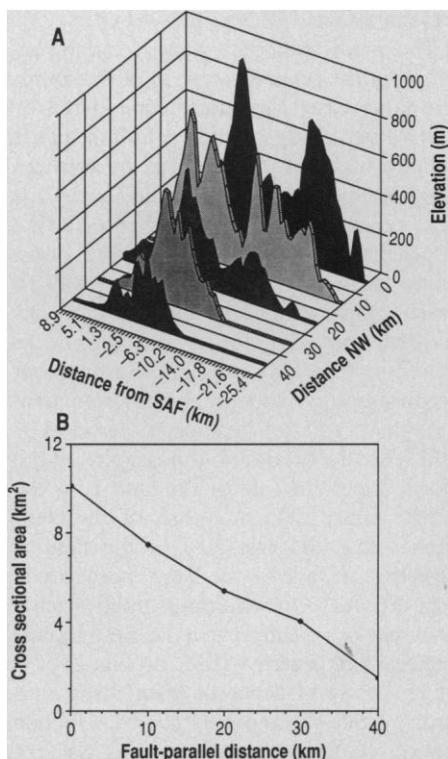


**Fig. 4.** (A) East-looking view of northern Santa Cruz Mountains topography shown at 10-km intervals starting at northwest edge of uplift pattern ( $y = 30$  km in Fig. 2). First profile crosses at Mount Bielawski, which is separated from Ben Lomond Mountain by the San Lorenzo River drainage. Note gradual decline in crestline altitude with northwest distance and deep incision of the topography by numerous stream systems crossed by these sections. The half-width of the topography (distance to a point at which the elevation is half of the crest height) on the fault-facing side is ~1 km, while that on the outboard side is ~10 km. (B) Cross-sectional area of the northern range evaluated at same sections depicted in (A). Note the monotonic decline (at roughly 3 to 5 km<sup>2</sup> per 10 km, or 2.4 to 4 km<sup>2</sup> per million years at a slip rate of 12.2 km per million years) as the range is subjected to geomorphic processes in the absence of further tectonic forcing.

3. G. C. P. King *et al.*, *ibid.* **93**, 13308 (1988); R. S. Stein *et al.*, *ibid.*, p. 13319.
4. This must be taken into account if the persistence time scale,  $\tau$ , for a bend of length  $\lambda$ , is large enough that  $U\tau > \lambda$ , where  $U$  is the long-term horizontal slip rate on the fault.
5. K. M. McNally *et al.*, *Eos* **70**, 1363 (1989).
6. G. Pfalker and J. P. Galloway, Eds., *U.S. Geol. Surv. Circ.* **1045** (1989), figure 8.
7. A. Aydin and B. M. Page, *Geol. Soc. Am. Bull.* **95**, 1303 (1983).
8. W. H. Prescott, M. Lisowski, J. C. Savage, *J. Geophys. Res.* **86**, 10,853 (1981).
9. S. P. Nishenko and P. L. Williams, *U.S. Geol. Surv. Open-File Rep.* OF85-0754 (1985).
10. W. C. Bradley and G. B. Griggs, *Geol. Soc. Am. Bull.* **87**, 433 (1976).
11. C. S. Alexander, *Univ. Calif. Publ. Geol.* **10**, 1 (1953).
12. T. C. Hanks *et al.*, *J. Geophys. Res.* **89**, 5771 (1984).
13. M. A. McKittrick, thesis, University of Arizona (1988).
14. G. E. Weber, in *Fieldtrip Guide to Coastal Tectonics and Coastal Hazards in Santa Cruz and San Mateo Counties, California*, G. E. Weber *et al.*, Eds. (Cordilleran Section, Geological Society of America 75th annual meeting, 1979), pp. 81–91.
15. J. M. Chappell, *Search* **14**, 99 (1983).
16. \_\_\_\_\_ and N. J. Shackleton, *Nature* **324**, 137 (1986).
17. D. Merritts and W. B. Bull, *Geology* **17**, 1020 (1989).
18. Latest values for the ages of the 5 a, c, e highstands from T. L. Ku *et al.*, *Quat. Res.* **33**, 129 (1990). The Santa Cruz terrace deposits cover two wavecut platforms [see (14)] in the town of Santa Cruz.
19. S. Y. Schwartz, D. L. Orange, R. S. Anderson, *Geophys. Res. Lett.*, in press.
20. J. C. Savage, quoted in (5).
21. Adapted from figure 3 in (5); updating of the plot provided by G. Valensise, personal communication. Uncertainty in the vertical scale of this pattern is largely due to the unknown height in the crust to which rupture occurred. Higher rupture will result in enhanced vertical displacement near the trace of the fault. The depicted pattern is based on a 5- to 6-km nearest approach of the rupture to the surface [see also (19)]. Confirmation of the gradient of the uplift pattern associated with the Loma Prieta event in the Santa Cruz coastal region is found in a single tilt measurement made by Applied Geomechanics, Inc., based in Live Oaks near Aptos, on the coast nearest the epicenter. They recorded 28  $\mu$ rad of tilt at an azimuth of 195° on their calibration instrument (F. Horath, personal communication), in close accord with the 25- $\mu$ rad gradient predicted in this area.
22. D. P. Schwartz and K. J. Coppersmith, *J. Geophys. Res.* **89**, 5681 (1984).
23. B. Bills and G. M. May, *ibid.* **92**, 11493 (1987).
24. W. R. Peltier, *Nature* **318**, 614 (1985); *J. Geophys. Res.* **91**, 9099 (1986).
25. L. M. Cathles III, *The Viscosity of the Earth's Mantle* (Princeton Univ. Press, Princeton, NJ, 1975).
26. Calculations based upon the following parameters:  $\rho_m - \rho_c = 500 \text{ kg/m}^3$ ;  $H = 4 \text{ km}$  [based on a choice of  $H_{\text{seismic}}/4$  for the elastic plate thickness (2)];  $E = 40 \text{ GPa}$ ;  $\nu = 0.25$  and formula for degree of compensation from D. Turcotte and G. Schubert, *Geodynamics* (Wiley, New York, 1982).
27. G. B. Griggs and J. R. Hein, *Geology* **88**, 541 (1980).
28. T. Best, personal communication.
29. W. H. Prescott and R. O. Burford, *Bull. Seismol. Soc. Am.* **66**, 1013 (1976).
30. E. A. Hay *et al.*, *Calif. Div. Mines Geol. Spec. Rep.* **140**, 41 (1980).
31. W. C. McLaughlin, *J. Res. U.S. Geol. Surv.* **2**, 593 (1974).
32. W. C. McLaughlin *et al.*, *U.S. Geol. Surv. Open-File Map* 88-752 (1988).
33. This hypothesis is detailed in (19).
34. A. C. Lawson *et al.*, *Carnegie Inst. Wash. Publ.* **87** (1908).
35. W. Thatcher, *Nature* **341**, 432 (1989).
36. B. M. Page and D. C. Engebretson, *Tectonics* **3**, 133 (1984).
37. The Ben Lomond fault bounding the east side of the mountain displays only minor displacement (~200 to 300 m of dip slip motion), and it occurred before the emplacement of the lower Pliocene Purisima Formation.
38. J. C. Clark, *U.S. Geol. Surv. Prof. Pap.* **1168** (1981).
39. This system has recently been modeled for the Southern Alps of New Zealand [P. O. Koons, *Am. J. Sci.* **289**, 1041 (1989)]. Adding to this complexity is the clear influence of lithology on the local stream system, demonstrated by the wrapping of the San Lorenzo and Pescadero drainages around the Salinian granitic core of Ben Lomond Mountain (Fig. 1).
40. See (19) for discussion of the uplift pattern expected from events on a southwest-dipping Sargent-Berrocal system.
41. I thank D. Orange, G. Griggs, G. Valensise, and G. King for discussions. I appreciate critiques of an earlier version of this manuscript by G. Valensise, M. Ellis, and D. Orange, and of later versions by D. Merritts and three anonymous reviewers. Terrace elevations were compiled by J. Buckthal. I thank the donors of the Petroleum Research Fund for partial support.

17 April 1990; accepted 6 June 1990

## A Molecular Ferromagnet with a Curie Temperature of 6.2 Kelvin: $[\text{Mn}(\text{C}_5(\text{CH}_3)_5)_2]^+ [\text{TCNQ}]^-$

W. E. BRODERICK, J. A. THOMPSON, E. P. DAY, B. M. HOFFMAN

The study of magnetic phase transitions in insulating molecular solids provides new insights into mechanisms of magnetic coupling in the solid state and into critical phenomena associated with these transitions. Only a few such materials are known to display cooperative magnetic properties. The use of high-spin molecular components would enhance intermolecular spin-spin interactions and thus a series of charge-transfer (CT) salts have been synthesized that utilize the spin  $S = 1$  molecular cation,  $[\text{Mn}(\text{C}_5(\text{CH}_3)_5)_2]^+$  (decamethylmanganocenium). The structure and cooperative magnetic behavior of  $[\text{Mn}(\text{C}_5(\text{CH}_3)_5)_2]^+ [\text{TCNQ}]^-$  (decamethylmanganocenium 7,7,8,8-tetracyano-*p*-quinodimethanide) are reported. This salt is a bulk molecular ferromagnet with the highest critical (Curie) temperature ( $T_c = 6.2 \text{ K}$ ) and coercive field ( $3.6 \times 10^3 \text{ gauss}$ ), yet reported for such a material.

THE SEARCH FOR MAGNETS comprised of discrete molecular components (1, 2) represents a new phase in an enterprise that began with the invention of the compass (3). However, to date only a small class of ferrimagnets (4) and a few well characterized bulk molecular ferromagnets are known: the halo-bis(dialkyl-dichalcogenocarbamato)iron(III) magnets (5) and  $[\text{Fe}(\text{C}_5(\text{CH}_3)_5)_2]^+ [\text{TCNE}]^-$  (decamethylferrocenium tetracyanoethylene) (6). Furthermore, these latter compounds contain iron, which is ferromagnetic in its elemental form and is the key component of lodestone (magnetite). We report that the donor-acceptor ( $[\text{D}]^+ [\text{A}]^-$ ) charge-transfer (CT) salt  $[\text{Mn}(\text{C}_5(\text{CH}_3)_5)_2]^+ [\text{TCNQ}]^-$  (I) (decamethylmanganocenium 7,7,8,8-tetracyano-*p*-quinodimethanide) is a true molecular ferromagnet and further propose that molecular ions with  $S \geq 1$ , such as  $[\text{Mn}(\text{C}_5(\text{CH}_3)_5)_2]^+$ , are particularly favorable for the preparation of magnetic molecular materials.

Directed synthesis of insulating ferromagnetic solids from molecular ions requires an

understanding of the mechanisms that stabilize the parallel alignment of the component spins. The energy of the ferromagnetic state can be written in the simplest case as a sum of the contributions from pairwise interactions between adjacent spins,  $E(F) = -\sum J_{ij} S_i S_j$ , where  $S_i$  and  $S_j$  are the spins of the adjacent interacting sites and  $J_{ij}$  is a coupling parameter for the interaction between them (1, 3, 7–10). The ground state is ferromagnetic if interactions that cause the spins of individual pairs to align parallel, corresponding to  $J_{ij} > 0$ , are dominant in three dimensions. Although such interactions include Heisenberg exchange for electrons in orthogonal orbitals (11), the most widely disseminated "prescription" (7) for generating pairwise ferromagnetic coupling in CT salts is based on a recognition by McConnell (1) that we may generalize as follows. Perturbative mixing into the ground state of an interacting  $[\text{D}]^+ [\text{A}]^-$  pair by a virtual CT excited state of the pair will selectively stabilize a ground state of the same spin multiplicity as the excited state. Thus ferromagnetism is favored by constituents for which the total spin angular momentum ( $S_T$ ) of the lowest-energy virtual CT state of an interacting  $\text{D}^+ \text{A}^-$  pair corresponds to the sum of the spins of  $\text{D}^+$  and  $\text{A}^-$ ,  $S_T = S(\text{D}^+) + S(\text{A}^-)$ ; antiferromagnetism (or ferrimagne-

W. E. Broderick, J. A. Thompson, B. M. Hoffman, Department of Chemistry and Materials Research Center, Northwestern University, Evanston, IL 60208.  
E. P. Day, Gray Freshwater Biological Institute, University of Minnesota, Navarre, MN 55392.